Acta Geotechnica (2021) 16:1161–1174
https://doi.org/10.1007/s11440-020-01031-6

RESEARCH PAPER

Monotonic and cyclic characteristics of K_0-Consolidated saturated soft clay under a stress path involving a variable confining pressure

Jun Wang[1,2,3] · Lei Wu[1,2,3] · Yuanqiang Cai[4] · Lin Guo[1,2,3] · Yunguo Du[5] · Changfei Gou[5] · Junfeng Ni[6] · Ziyang Gao[6]

Received: 18 July 2019 / Accepted: 13 July 2020 / Published online: 27 October 2020

Abstract
In certain field conditions such as offshore projects under wave loads or embankments under traffic loads, both the vertical and horizontal stresses are variable. However, previous investigations rarely considered the variation in horizontal stress. To better understand the characteristics of natural saturated soft clay, a series of monotonic and cyclic triaxial tests with a K_0-consolidation state were carried out under a variable confining pressure (VCP) stress path. The development of axial strain, pore water pressure and effective stress path is analysed. The results show that with the increase in η (the ratio of the variation in the mean effective principal stress to that of the deviatoric stress), the undrained shear strength (q_f) decreases continuously. The pore water pressure generation is slightly improved under a stress path with increasing confining pressure. Based on the test results, a unified formula was established to predict the pore water pressure under VCP stress paths. The unique p–q–e relationship of normally consolidated clay in monotonic VCP triaxial tests was also demonstrated. Under VCP stress paths, the amplitude of the pore pressure increases, and the effective stress path tilts more sharply to the right. Moreover, a unified formula was established that can provide a good reference for predicting effective stress paths under cyclic VCP triaxial tests.

Keywords K_0-consolidation · Soft clay · Triaxial test · Variable confining pressure

1 Introduction

Natural soft clay is widely distributed in the coastal areas of China, and many projects, such as highways, railways and airport runways, have been built on this kind of soil foundation. Both the vertical and horizontal stresses vary in many actual engineering projects, such as offshore projects under wave loads or embankments under traffic loads [2]. It is very difficult to precisely predict deformation because the variation in only the vertical stress is considered in most of the existing studies. To solve this problem, the monotonic and cyclic behaviour of saturated soft clay based on stress paths involving variations in both the vertical and horizontal stresses should be investigated.

In the past few decades, many scholars have investigated the monotonic and cyclic behaviour of saturated soft clay in triaxial tests [8, 10, 17, 18]. Constant confining pressure (CCP) is commonly used in these triaxial tests, and the variation in only vertical stress can be considered. The actual stress path of the soil in an engineering project

✉ Lin Guo
lingpray@126.com

1 College of Architecture and Civil Engineering, Wenzhou University, Chashan University Town, Wenzhou 325035, China

2 Key Laboratory of Engineering and Technology for Soft Soil Foundation and Tideland Reclamation of Zhejiang Province, Wenzhou, China

3 Innovation Centre of Tideland Reclamation and Ecological Protection, Wenzhou University, Wenzhou, Zhejiang 325035, China

4 Department of Civil Engineering, Zhejiang University of Technology, Hangzhou 310014, China

5 Wenzhou Mass Transit Railway Investment Group Co., LTD, Wenzhou 325035, People's Republic of China

6 Department of Civil Engineering and Architecture, Saga University, Saga, Japan

may be very different from the stress path provided by CCP triaxial tests because the variation in horizontal stress is not considered with CCP.

With the development of experimental apparatuses, triaxial tests with variable confining pressure (VCP) were conducted recently to simulate the variation in horizontal stress. Compared with the CCP triaxial tests, the VCP triaxial tests can more accurately simulate the actual state by simultaneously controlling the cyclic variation in both the vertical deviatoric stress and confining pressure. Currently, some VCP triaxial test investigations have been performed on the behaviour of soil [4, 12–14, 16, 19, 21]. Nataatmadja and Parkin [12] conducted experimental research on broken rock and found that the value of the rebound modulus from the CCP test is higher than that from the VCP test. Wichtmann et al. [19] studied the influence of the VCP stress path on the unidirectional drainage characteristics of saturated sand and noted that the coupling of the cyclic confining pressure and cyclic deviatoric stress changed not only the strain development rate but also the strain development direction. Rondón et al. [13] conducted a series of CCP and VCP tests on unbound granular materials, focusing on the cumulative deformation characteristics. The results show that the cumulative axial strain and bulk strain are similar under certain stress paths. The CCP tests underestimated the development of cumulative axial strain compared to the VCP tests under the other stress paths. However, most of the existing studies that utilized VCP tests focused on the rebound characteristics of coarse-grained material. Few experiments of saturated soft clay under a VCP stress path were carried out.

Cai et al. [2] and Gu et al. [5–7] studied the cyclic characteristics of soft clay from Wenzhou, China, under VCP stress paths. Gu et al. [5] designed stress paths to simulate the coupling effects of the varying shear and normal stresses in clays resulting from earthquakes or other vibration sources and then found that VCP tests are more appropriate than CCP tests for simulating in situ stress fields in terms of strong P-wave propagation in soil layers. Gu et al. [7] investigated the coupling effects of both the cyclic shear stress and cyclic normal stress on the $G/G_{\max}$ characteristics of saturated clays through cyclic triaxial tests under VCP. Cai et al. [2] found that the VCP is vital to elucidate the one-way behaviour of saturated clay. However, in all these studies, the soil specimens were isotropically consolidated. Virtually, during in situ sedimentary processes, marine clay deposits are mainly in a K_0-consolidation state [10]. Andersen et al. [1] first conducted cyclic triaxial tests on K_0-consolidated clays. However, due to the limits of experimental conditions, the K_0 state was approximately controlled by the ratio of the horizontal stress to the vertical stress, which results in a limit to the test numbers. Guo et al. [9] presented systematic cyclic HCA tests including parallel cyclic CCP triaxial tests on K_0-consolidated saturated soft clay. In general, studies of the monotonic and cyclic behaviour of natural K_0-consolidated soft clay under a VCP stress path remain limited.

Considering the true consolidation state of natural soft clay, the cyclic characteristics of K_0-consolidated soft clay are further studied in this paper to reveal the coupling effects of cyclic confining pressure and cyclic deviatoric stress on the properties of natural soft clay. A series of monotonic and cyclic VCP triaxial tests are conducted. The development of axial strain, pore water pressure and effective stress path is analysed. Based on the test results, a unified formula was established that can provide a good reference for predicting effective stress paths under cyclic VCP triaxial tests.

2 Sampling method and soil properties

The soft marine clay tested in this paper is obtained from Wenzhou, Zhejiang Province, China. This type of clay is typically 30–100 m thick and has been recognized as one of the most problematic soils in China due to its remarkable characteristics of high water content, high compressibility, low permeability and low bearing capacity. The authors' research group [3, 5, 8, 9] and many other researchers [10] have previously conducted several investigations on this kind of soft clay.

A test pit with a depth of approximately 3 m was excavated at a site 2 km away from the Wenzhou Longwan Airport to obtain undisturbed clay samples. The groundwater level at this site is approximately 0.8 m below the ground surface. The criteria recommended by [11] are applicable to Wenzhou clays which means the soil sample is almost undisturbed. The index properties of the soft clay used are shown in Table 1.

Table 1 Index properties of the tested soft clay

Index properties	Value
Specific gravity, G_s (g/cm^3)	2.69
Natural water content, w_n (%)	56–59
Initial density, ρ_0 (g/cm^3)	1.65–1.68
Initial void ratio, e_0	1.55–1.59
Liquid limit, w_L (%)	64
Plasticity index, I_p	36
Clay fraction (%)	41
Silt fraction (%)	55
Permeability coefficient, k_v (cm/s)	2.5×10^{-6}

3 Test apparatus and procedures

The apparatus used in this study is a DYNTTS manufactured by GDS Instruments Ltd., U.K. The specimens were in a diameter of 50 mm and a height of 100 mm. Then, the specimen was saturated under a backpressure that was applied in three levels (100 kPa, 200 kPa and 300 kPa) for 24 h with an effective confining pressure of 10 kPa to guarantee that the B value was greater than 0.98 in all tests. During K_0-consolidation, axial stress was adjusted continuously to ensure the vertical displacement equal to the drainage volume divided by the cross-sectional area of the specimen. Thus, there is no lateral deformation in K_0-consolidation. In this paper, the axial stress was σ_1^0 = 74.5 kPa, which was greater than the overburden pressure of 67 kPa, and the confining pressure was σ_3^0 = 41 kPa. Therefore, the K_0 value approximately equals 0.55 which is the same with the K_0 value of Wenzhou clay in [10].

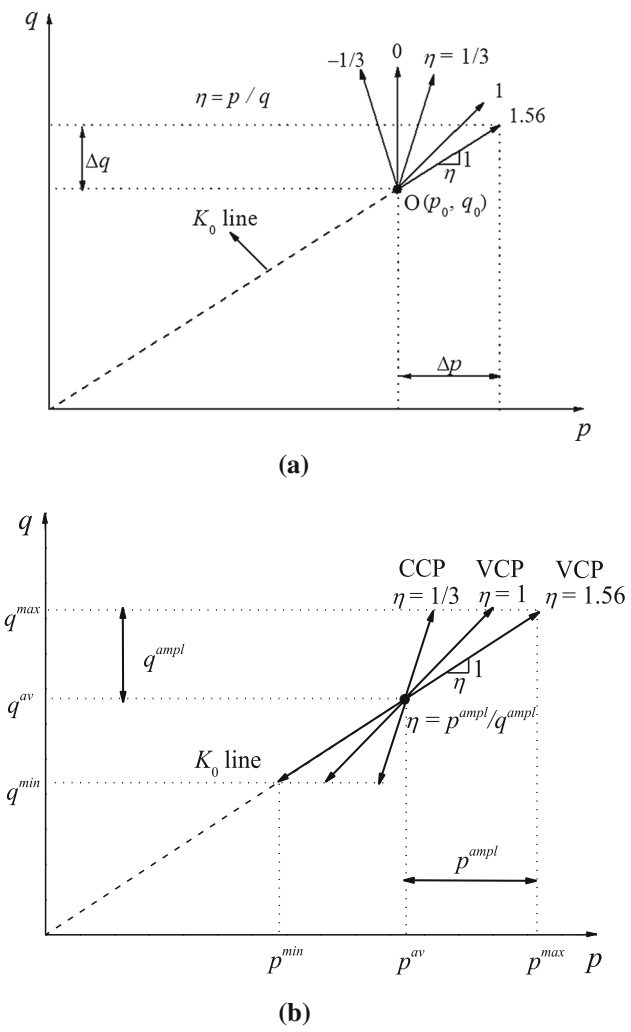

Fig. 1 Schematic diagrams of the applied triaxial tests under VCP in (**a**) monotonic tests; **b** cyclic tests

The loading procedures of monotonic tests are shown in Fig. 1a. In addition, the initial mean effective principal stress p_0 and the initial deviatoric stress q_0 in p-q space can be calculated as follows:

$$p_0 = \left(\sigma_0^1 + 2\sigma_0^3\right)/3 \tag{1}$$

$$q_0 = \sigma_0^1 - \sigma_0^3 \tag{2}$$

Therefore, the initial mean effective principal stress was p_0 = 52.2 kPa, and the initial deviatoric stress was q_0 = 33.5 kPa.

During the monotonic tests, the axial stress and the confining pressure acting on the specimens changed simultaneously. The variation in the effective principal stress and the deviatoric stress can be calculated by the following formulas:

$$p = (\sigma_1 + 2\sigma_3)/3 \tag{3}$$

$$q = \sigma_1 - \sigma_3 \tag{4}$$

The ratio of the variation in the effective principal stress to that of the deviatoric stress was defined as η:

$$\eta = p/q = [(\sigma_1 + 2\sigma_3)/3]/q = 1/3 + \sigma_3/q \tag{5}$$

In the CCP tests, $\eta \equiv 1/3$, because the confining pressure was constant. In the VCP tests, when the confining pressure increased, $\eta > 1/3$. Otherwise, $\eta < 1/3$. Five values of η (η = -1/3, 0, 1/3, 1, 1.56) were applied in monotonic tests. The loading rate of the deviatoric stress was 0.1 kPa/min. The tests were ended when the axial strain reached 20%.

Likewise, the loading procedures of cyclic tests are shown in Fig. 1b. The axial stress (amplitude σ_1^{ampl}) continuously changed during the cyclic tests, as did the confining pressure (amplitude σ_3^{ampl}) at the same time. Furthermore, the amplitudes of the mean effective principal stress and the deviatoric stress can be calculated as follows:

$$p^{\text{ampl}} = (\sigma_1^{\text{ampl}} + 2\sigma_3^{\text{ampl}})/3 \tag{6}$$

$$q^{\text{ampl}} = \sigma_1^{\text{ampl}} - \sigma_3^{\text{ampl}} \tag{7}$$

The ratio of the amplitude of mean effective principal stress to that of the deviatoric stress was defined as η_{cyc} which can represent the direction of the effective stress path in Fig. 1b:

$$\eta_{\text{cyc}} = p^{\text{ampl}}/q^{\text{ampl}} = \left[\left(\sigma_1^{\text{ampl}} + 2\sigma_3^{\text{ampl}}\right)/3\right]/q^{\text{ampl}} = 1/3 + \sigma_3^{\text{ampl}} + q^{\text{ampl}} \tag{8}$$

Gu et al. [5] once used the results at the frequency of 0.001 Hz to verify the measured results with f = 0.1 Hz for WZ-A clay and found the results were similar to each other. Furthermore, the low frequency is able to better

capture the pore pressure reaction, and the results are more realistic [23]. Hence, a frequency of 0.001 Hz was applied in cyclic loading. There were a total of nine tests in this group. The amplitudes of the cyclic deviatoric stress were 10 kPa, 15 kPa and 20 kPa, respectively. Then, three values of CSR (CSR = 0.10, 0.14, 0.19), which is defined as CSR = $q_{cyc}/(2p_0')$, and three values of η_{cyc} (η_{cyc} = 1/3, 1, 1.56) were applied to the specimens in the tests.

4 Test results and discussion

4.1 Monotonic tests

Figure 2 illustrates different values of the axial stress σ_1 and the confining pressure σ_3, respectively. It shows that the GDS triaxial test system loads steadily and the stress precision is relatively high.

The curves of deviatoric stress versus axial strain under different stress paths can be seen in Fig. 3a. During the initial loading stage, the deviatoric stress increases more rapidly with increasing axial strain. The deviatoric stress remains steady when the axial strain is greater than 10%; meanwhile, the axial strain continuously increases to 20%. Due to the end effect, when the axial strain is relatively large (greater than 10%), the top-down deformation of the soil will begin to become inhomogeneous, causing the central part of the specimen to slightly bulge during the compression process. The mean stress–strain relationship obtained at this time cannot fully reflect the true stress–strain state of the soil. Consequently, the deviatoric stress corresponding to the axial strain of 10% can be taken as the shear strength (q_f) of the specimen.

As shown in Fig. 3b, with the increase in η, q_f decreases continuously. The corresponding values of q_f are 55.7 kPa, 53.8 kPa, 52.9 kPa, 51.2 kPa and 48.9 kPa when the values of η are −1/3, 0, 1/3, 1 and 1.56, respectively. There are obvious differences between the strength of soil under different stress paths (the strength of η = 1.56 is 13% lower than that of η = −1/3). These results may be attributed to the reduction in effective stress, which is associated with lower strength. As η increases, the pore water pressure increases, which then leads to a decrease in the effective stress. Hence, in the analysis of practical engineering problems, the strength parameters should be determined more accurately according to the true stress path of the soil.

Figure 4 shows the variability in the curves of pore water pressure versus axial strain under different stress paths. At the initial loading stage, all of the pore pressures under different stress paths increase with the axial strain. When the axial strain is 10%, the pore pressure of η = 1.56

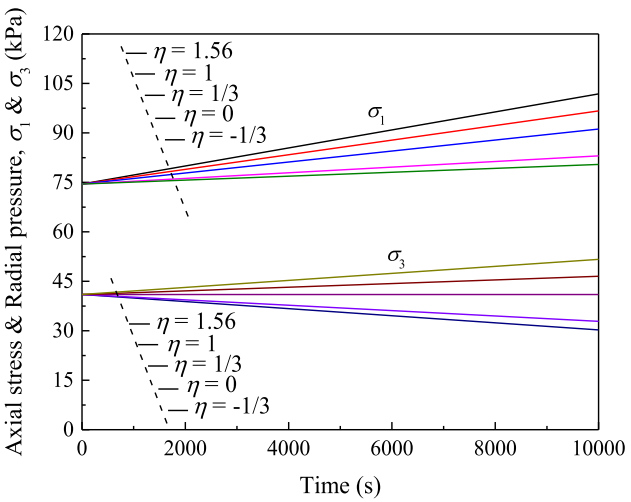

Fig. 2 Curves of stress versus time

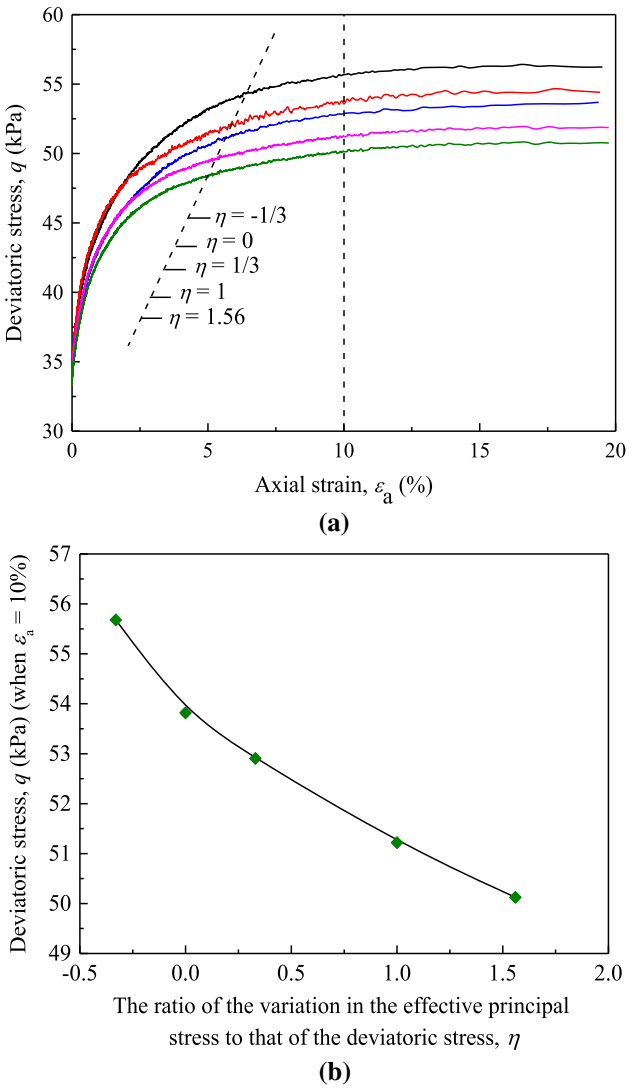

Fig. 3 **a** Curves of deviatoric stress versus axial strain under different stress paths; **b** the relationship between q (when ε_a = 10%) and η (η = − 1/3, 0, 1/3, 1, 1.56)

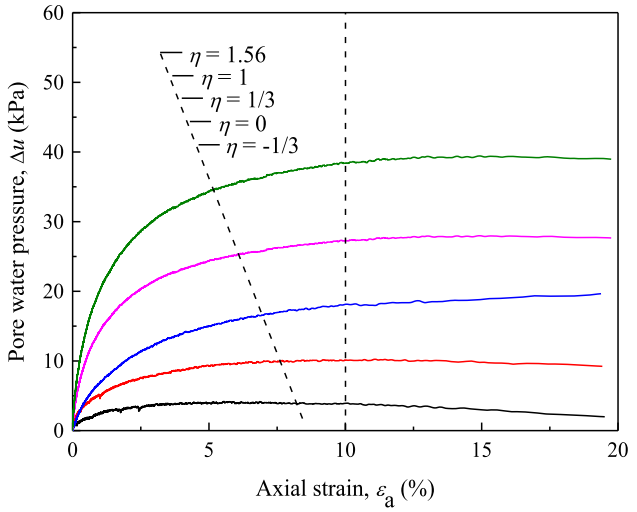

Fig. 4 Curves of pore water pressure versus axial strain under different stress paths

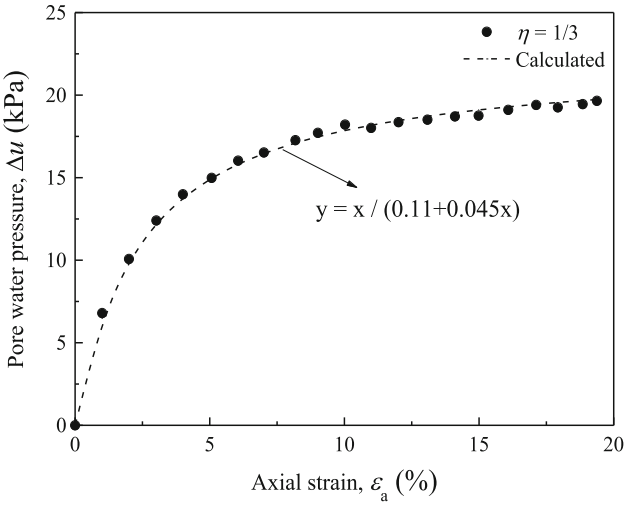

Fig. 5 Formula of pore pressure versus axial strain under CCP

is 112% larger than that in CCP (η = 1/3) test. When the axial strain is larger than 10%, the pore pressure remains constant ($\eta \geq 1/3$) or decreases ($\eta < 1/3$) with increasing axial strain. At the same time, the deformation of the specimen develops rapidly and is inhomogeneous. The pore pressure at this time may be distorted.

Compared with the results of the conventional triaxial test (CCP, η = 1/3), the pore water pressure generated by the specimen under stress paths with increasing confining pressure slightly increases. In contrast, while the specimens were under stress paths with decreasing confining pressure, the produced pore water pressure decreases because the pore water pressure in the monotonic tests partially results from the variation in the deviatoric stress and partially arises from the change in the confining pressure. In terms of the conventional triaxial tests (η = 1/3), since the value of the confining pressure is constant, the pore water pressure is generated by the variation in the deviatoric stress only. Yasuhara et al. [20] analysed the experimental results of triaxial compression tests of specimens under CCP; then, the following relationship between pore water pressure and axial strain was obtained:

$$\Delta u_{(\eta=1/3)} = \frac{\varepsilon_a}{a + b\varepsilon_a} \tag{9}$$

The calculation formula of pore water pressure and axial strain under CCP is illustrated in Fig. 5. Fitting the test results with Formula (9), a = 0.11 and b = 0.045 can be obtained. Formula (9) can accurately express the relationship between pore water pressure and axial strain under the CCP stress path.

In addition, the pore water pressure that results from the variation in confining pressure can be calculated by using Skempton theory [15]:

$$\Delta u_{\sigma_r} = B\Delta\sigma_r \tag{10}$$

In this paper, the value of B is approximately 0.98.

By combining Formula (9) and Formula (10), a unified expression of pore water pressure can be obtained:

$$\begin{aligned}\Delta u &= \Delta u_{(\eta=1/3)} + \Delta u_{\sigma_r} = \frac{\varepsilon_a}{a + b\varepsilon_a} + B\Delta\sigma_r \\ &= \frac{\varepsilon_a}{a + b\varepsilon_a} + B\eta\Delta q\end{aligned} \tag{11}$$

Figure 6 shows the prediction of the pore water pressure under different stress paths through Formula (11). It can be concluded that the calculated results are in good agreement with the measured data, especially when the axial strain is lower than 10%.

The stress paths of the K_0-consolidated undrained triaxial tests are illustrated in Fig. 7. Under different total

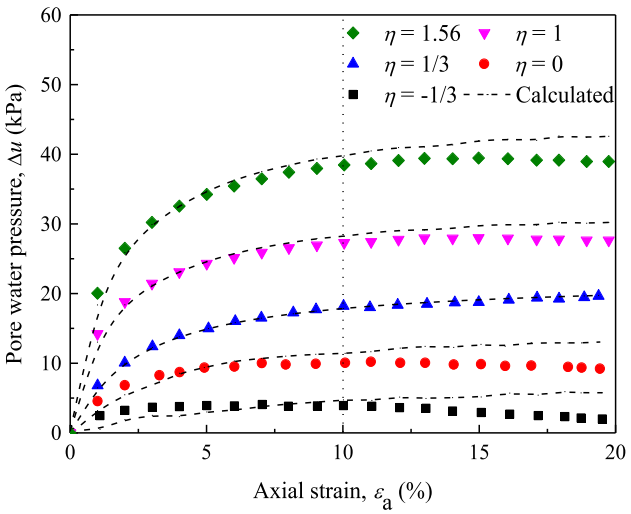

Fig. 6 Comparison between the measured and the predicted pore pressures

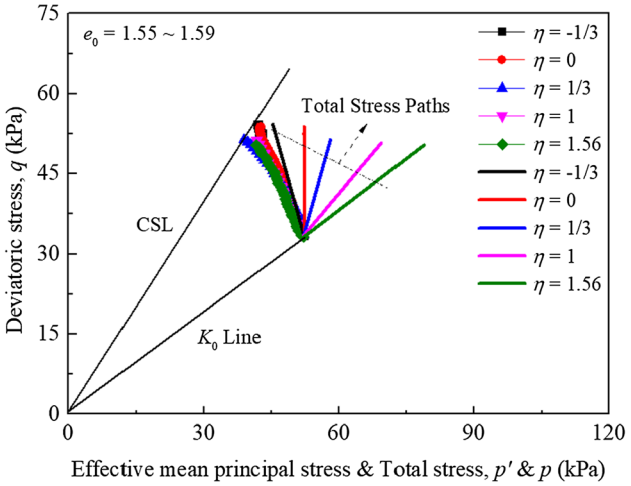

Fig. 7 Stress paths of K_0-consolidated undrained triaxial monotonic tests under VCP

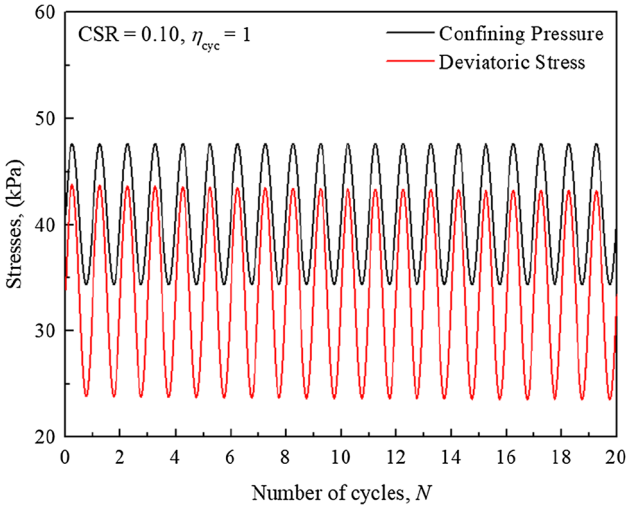

Fig. 8 Variation in the cyclic loading stress under different stress paths with the number of cycles (CSR = 0.10, η_{cyc} = 1)

stress paths, the effective stress paths are basically the same. This is because under the same deviatoric stress, the pore pressure is produced by the variable confining pressure only and the formation of pore pressure offsets the variation in confining pressure (Skempton, Formula (10)). Zeng and Chen [22] highlighted the unique *p*–*q*–*e* relationship of normally consolidated clay. That is, as to the specimens with the same void ratio (e) in the undrained tests, the volume of the soil keeps constant during the shear process, corresponding to the unique effective stress path on the state boundary surface, which is independent of the total stress path. These test results demonstrate that, in terms of K_0-consolidated saturated soft clay, within the range of $-1/3 < \eta < 1.56$, the unique *p*–*q*–*e* relationship of normally consolidated clay is still valid.

4.2 Cyclic tests

4.2.1 Loading stresses under VCP

When CSR = 0.10, as shown in Fig. 8, the cyclic loading stresses of different stress paths varied with the number of cycles. The cyclic deviatoric stress was cyclically applied in the form of a sine wave with an amplitude q^{ampl} = 10 kPa. The confining pressure under VCP tests changed in the form of a sine wave as well. The amplitude of that can be calculated as follows:

$$\sigma_3^{ampl} = q^{ampl}(\eta_{cyc} - 1/3) \tag{12}$$

That is, when η_{cyc} = 1, the amplitude of the confining pressure was $\sigma_3^{ampl} = 6.7\mathrm{kPa}$. When η_{cyc} = 1.56, it was $\sigma_3^{ampl} = 12.3\mathrm{kPa}$.When CSR = 0.14 and 0.19, the loading stress–time curves were similar to those shown in Fig. 8; however, when CSR = 0.14, the amplitude of the cyclic deviatoric stress was q^{ampl} = 15 kPa. When CSR = 0.19, q^{ampl} = 20 kPa. The amplitude of the confining pressure can be calculated from Formula (12).

4.2.2 Development of cyclic pore pressure

Figure 9 illustrates the development trends of pore water pressure under different stress paths with the number of cycles. It is evident that despite the differences in both the CSRs and stress paths, the pore pressure increases with the number of cycles. In particular, the pore pressure increases rapidly in the early stage of loading and gradually stabilizes after at least 15 loops. The cyclic variation in confining pressure has approximately the same effect on the pore pressure under different CSRs. With the increasing value of η_{cyc}, the amplitude of the cyclic confining pressure increases, as does the vibration amplitude of the pore pressure. When η_{cyc}= 1 and 1.56, the amplitudes are about 2.5 and five times larger than that in CCP (η_{cyc}= 1/3) tests.

The pore pressure under cyclic loading can be divided into the stress pore pressure (elastic pore pressure), the structural pore pressure (residual pore pressure) and the transitive pore pressure according to its causes and characteristics [24]. The stress pore pressure is a recoverable part of the pore pressure caused by the generation of the elastic volumetric strain potential energy of the soil skeleton. The structural pore pressure is an unrecoverable part of the pore water pressure caused by the generation of the plastic volumetric strain potential energy of the failure of the soil skeleton. The transitive pore pressure is the corresponding part of the variation in the volumetric strain potential energy of the soil skeleton caused by the flowing of the pore water. The pore pressure can be represented as:

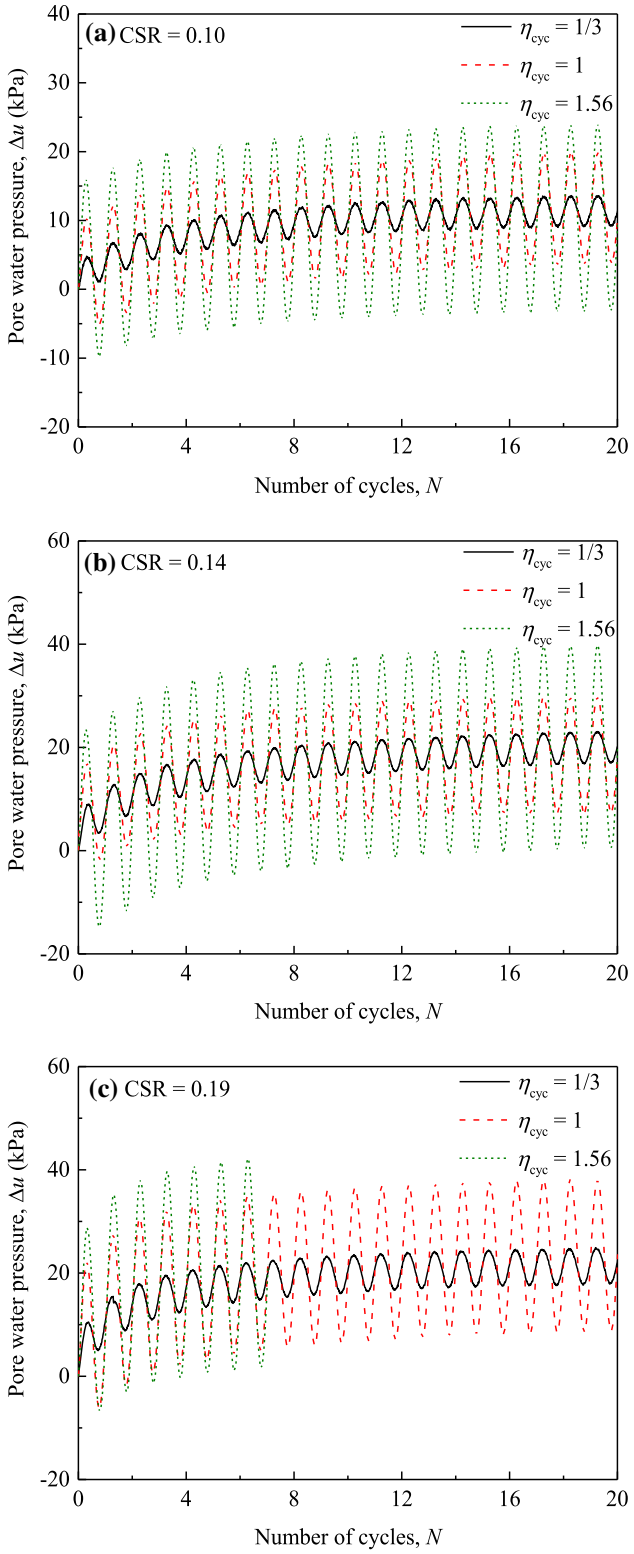

Fig. 9 Development of pore water pressure under different stress paths with the number of cycles: **a** CSR = 0.10; **b** CSR = 0.14; **c** CSR = 0.19

$$u(t+\Delta t) = u(t) + \Delta u = u(t) + \Delta u_\sigma + \Delta u_p + \Delta u_T \qquad (13)$$

where Δu_σ, Δu_p and Δu_T are the elastic pore pressure, the residual pore pressure and the transitive pore pressure, respectively.

As shown in Fig. 9, the residual pore pressures of the specimens under different stress paths are similar. The cyclic variation in the confining pressure mainly leads to the change in the instantaneous elastic pore water pressure. The transitive pore pressure will not be discussed in this paper due to its multifarious and complicated causes. The residual pore pressure and the elastic pore pressure of different stress paths are analysed as follows:

(1) Residual pore pressure

At a low frequency of 0.001 Hz, the strain and pore pressure reactions are relatively in time during the loading process. Hence, the strain and the pore pressure of each specimen can be considered as the residual strain and the residual pore pressure after each cycle. The development trends of the residual pore pressure under different CSRs and different stress paths with the number of cycles are presented in Fig. 10. The residual pore pressure continues growing with increasing CSR. Although the stress paths are different, the relationships between the residual pore pressure and the number of cycles under the same value of CSR show roughly the same tendency.

Notably, under the same CSR, such as 0.10, the relationship between the residual pore pressure and the number of cycles is approximately hyperbolic, which can be presented according to the form of the hyperbolic model:

$$\Delta u_p = \frac{N}{a + bN} \qquad (14)$$

Using Formula (14), a regression analysis of the data in Fig. 10 was conducted to obtain the parameters a and b. Therefore, when CSR = 0.10, 0.14 and 0.19, respectively,

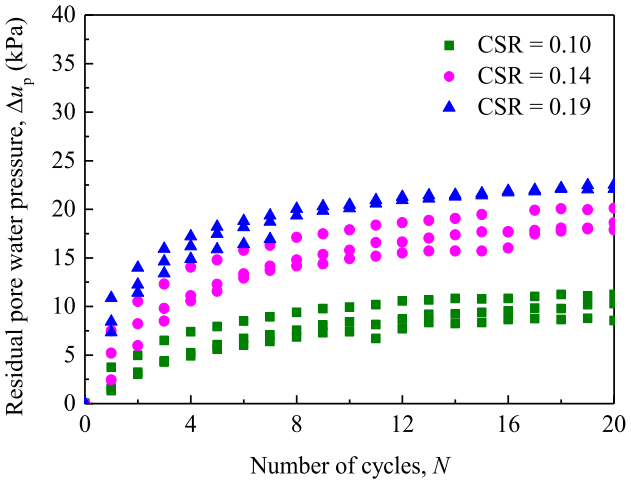

Fig. 10 Development of the residual pore pressure under different stress paths with the number of cycles

$$\Delta u_p = \frac{N}{0.36349 + 0.0809N} \tag{15}$$

$$\Delta u_p = \frac{N}{0.15417 + 0.0461N} \tag{16}$$

$$\Delta u_p = \frac{N}{0.08052 + 0.04113N} \tag{17}$$

By comparing the predictions of Formulas (15)–(17) with the test results, as shown in Fig. 11, it is found that the larger the CSR value, the more accurate the prediction is. When CSR = 0.19, the correlation coefficient is 0.98125, which means that a good prediction is provided by Formula (17).

By combining Formulas (15)–(17), a unified expression of residual pore pressure can be obtained:

$$\Delta u_p = \frac{N}{(41.78CSR^2 - 15.26CSR + 1.47) + (8.56CSR^2 - 2.92CSR + 0.29)N} \tag{18}$$

(2) Elastic pore pressure

As mentioned above, the elastic pore pressure is greatly influenced by the cyclic confining pressure. According to Skempton theory [15], for saturated soil, a variation in the mean principal stress generates an equivalent excess pore water pressure. Figure 9 shows that the residual pore pressure remained almost unchanged after 15 loops. During this period, the majority of the pore pressure generated by the variation in average principal stress can recover after cyclic loading. The pore pressure at this moment is considered approximately elastic:

$$\Delta u_\sigma = B \times \Delta p \tag{19}$$

where B is the pore pressure coefficient. In this study, B was measured to be 0.98.

Combined with Formula (8), the elastic pore pressure can be calculated by the following formula:

$$\Delta u_\sigma(\eta) = \eta_{\mathrm{cyc}} B q^{\mathrm{ampl}} \tag{20}$$

Then, the instantaneous increment of pore pressure caused by the variation in confining pressure is as follows:

$$\Delta u_\sigma(\sigma^{\mathrm{ampl}}) = \Delta u_\sigma(\eta) - \Delta u_\sigma(1/3) = (\eta_{\mathrm{cyc}} - 1/3) B q^{\mathrm{ampl}} \tag{21}$$

For example, when CSR = 0.10, the maximum pore pressures in the 20th loop are 13.59 kPa, 20.01 kPa and 23.97 kPa, corresponding to the three stress paths with η_{cyc} = 0.33, 1 and 1.56, respectively. The corresponding residual pore pressures are 11.21 kPa, 10.27 kPa and 8.53 kPa. Therefore, the pore pressure increments of the 20 loops are 2.38 kPa, 9.74 kPa and 15.44 kPa, respectively. The instantaneous increment of pore pressure caused by the variation in confining pressure is 7.36 kPa when η_{cyc} = 1 but 13.06 kPa when η_{cyc} = 1.56. Compared with the value calculated by Formula (21): when η_{cyc} = 1, $\Delta u_\sigma\left(\sigma_3^{ampl}\right) = (1 - 1/3) \times 0.98 \times 10 = 6.53\mathrm{kPa}$, and the error is 11.3%. When η_{cyc} = 1.56, $\Delta u\left(\sigma_3^{ampl}\right) = (1.56 - 1/3) \times 0.98 \times 10 = 12.02\mathrm{kPa}$, and the error is 8.0%.

Due to the insufficient response of pore pressure during the test, one coefficient α is adapted to adjust the elastic pore pressure value.

In summary, the total pore pressure in a cyclic triaxial test under VCP can be calculated as follows:

$$\begin{aligned}\Delta u &= \Delta u_\sigma + \Delta u_{\mathrm{p}} \\ &= \alpha \eta_{\mathrm{cyc}} B q^{\mathrm{ampl}} + \frac{N}{(41.78\mathrm{CSR}^2 - 15.26\mathrm{CSR} + 1.47) + (8.56\mathrm{CSR}^2 - 2.92\mathrm{CSR} + 0.29)N}\end{aligned} \tag{22}$$

According to the experimental conditions in this study, taking 0.8 as the value of α is suitable. Taking CSR = 0.19 as an example, the predictions of pore water pressure in Fig. 12 are based on Formula (22). Figure 12 shows that the predicted results fit the development trend of the pore pressure in general, although there are still some deviations. According to Fig. 11, it is worth noting that the

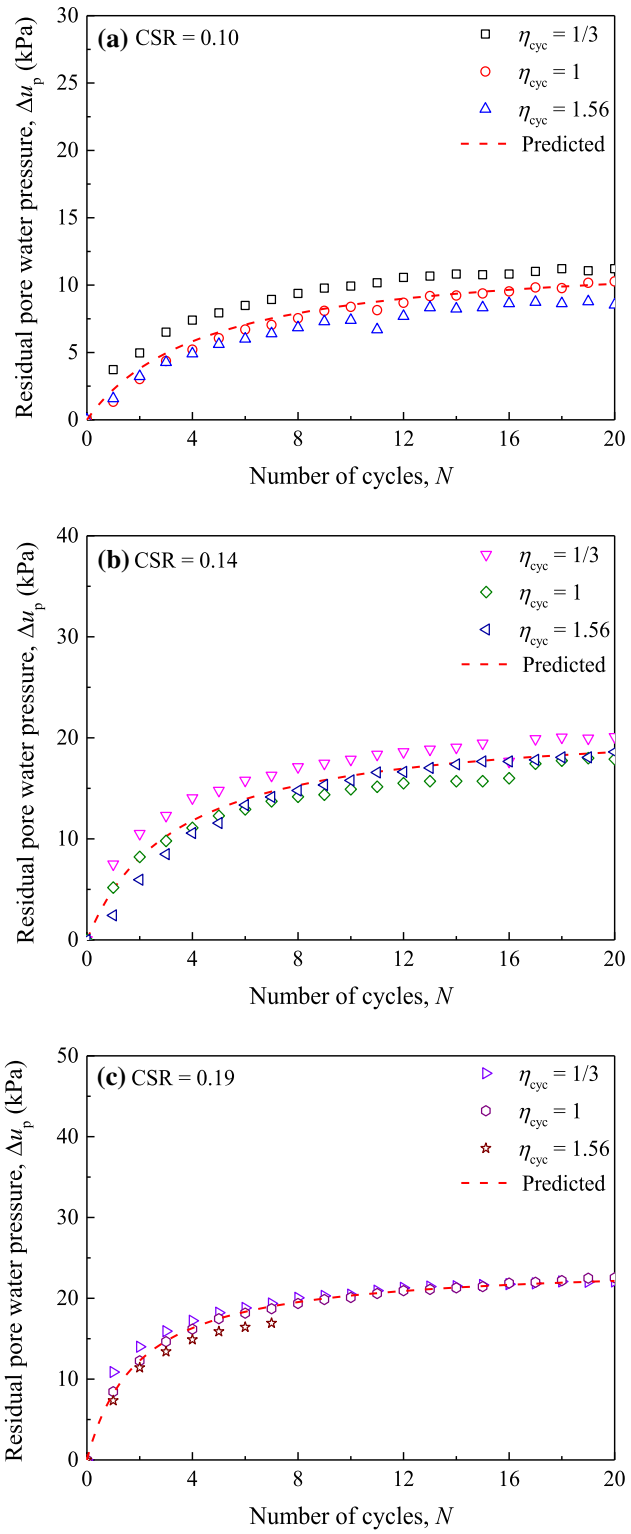

Fig. 11 Comparison between the prediction and the test results: **a** CSR = 0.10; **b** CSR = 0.14; **c** CSR = 0.19

greater the CSR value is, the more accurate the predicted results are. On the one hand, since the value of the transitive pore pressure is not calculated, a difference between the predicted results and the experimental results exists. On the other hand, the calculated value of residual pore pressure obtained from Formula (18) may not be sufficiently accurate.

4.2.3 Analysis of effective stress paths under VCP

The development pattern of the effective stress path depends on the total stress path and the instantaneous pore pressure. Based on the discussion about the elastic pore pressure mentioned above, the development of pore pressure is greatly influenced by the cyclic confining pressure; therefore, the development of an effective stress path is distinctive under different stress paths.

Figure 13 presents the total stress paths and corresponding effective stress paths with different CSRs in the VCP cyclic loading tests. When η_{cyc} = 1/3 (CCP), in the first few cycles, due to the continuous accumulation of pore pressure, the effective stress path (the red line) develops towards the direction (left) in which the mean effective stress decreases. As the number of cycles becomes larger, the accumulation of the pore pressure becomes low enough such that the effective stress paths almost overlap. Then, the final effective stress path slightly tilts to the right. In addition, during a single cycle, the amplitude of the pore pressure variation becomes small. Consequently, due to the slight variation in the pore pressure while loading or unloading, the effective stress path is almost a straight line. When η_{cyc} = 1 and 1.56 (VCP), the effective stress paths also develop towards the direction in which the mean effective stress decreases and then become stable after more cycles. Nevertheless, because of the simultaneous variations in both the confining pressure and cyclic deviatoric stress, the amplitudes of the pore pressure become larger, and the effective stress paths tilt more evidently to the right. Furthermore, during a single cycle, the amplitudes of the pore pressure change more intensely while loading or unloading, so the effective stress paths are no longer straight lines; instead, they cover a certain area.

Compared with CSR = 0.10, the effective stress paths of the specimens under different stress paths vary considerably with increasing CSRs. In particular, when CSR= 0.19, due to the large axial deformation, the cyclic deviatoric stress somewhat decays with the increasing number of cycles while loading. When CSR = 0.19 and η_{cyc} = 1.56,

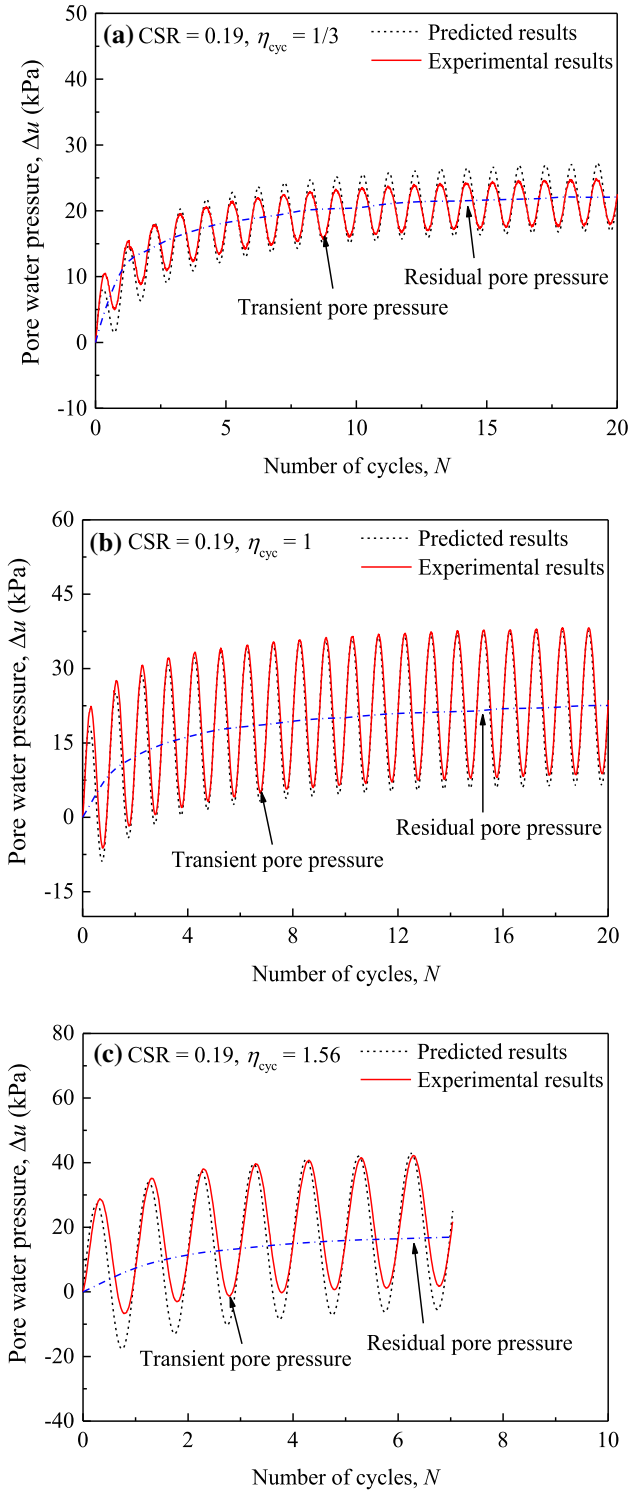

Fig. 12 Comparison between the predicted and experimental results (CSR = 0.19): **a** η_{cyc} = 1/3; **b** η_{cyc} = 1; **c** η_{cyc} = 1.56

this phenomenon is most evident (Fig. 13(i)), and the specimens failed after just seven cycles.

The predictions of effective stress paths with different CSRs under VCP are calculated on the basis of the predicted pore pressure results, which are partially shown in Fig. 14. The deviatoric stress and confining pressure are simulated through the sine waveform, as plotted in Fig. 8. Notably, the greater the CSR value is, the more accurate the predictions are. When CSR = 0.19, to some extent, the predicted effective stress paths are roughly consistent with the development of the experimental results, although there are still some deviations, especially when η_{cyc} = 1/3 and 1.

5 Conclusions

In this paper, K_0-consolidated saturated soft clay specimens were tested under VCP stress paths. Five values of η (η =− 1/3, 0, 1/3, 1, 1.56) were applied in the monotonic tests. In addition, cyclic loading of three stress paths (η_{cyc}=1/3, 1, 1.56) under three CSRs was applied at a frequency of 0.001 Hz. The conclusions are listed as follows:

(1) In monotonic tests, the strength of K_0-consolidated saturated soft clay continuously decreases 13% with the increase in η. Thus, the strength parameters should be determined accurately according to the true total stress path. However, because the formation of pore pressure in saturated soft clay offsets the variation in confining pressure under the same deviatoric stress, the effective stress paths are basically identical.

(2) Compared with the results of conventional monotonic triaxial tests, the pore water pressure generation is improved under a stress path with increasing confining pressure. When η = 1.56, it is 112% larger than that in CCP test. A unified formula to predict the pore water pressure was established under VCP stress paths.

(3) In cyclic tests under different CSRs, the amplitude of the pore pressure increases with η_{cyc}. When η_{cyc} = 1 and 1.56, the amplitudes are about 2.5 and 5 times larger than that in CCP (η_{cyc} = 1/3) tests. Based on the elastic pore pressure formula, a formula for the total pore pressure in VCP cyclic triaxial tests was obtained.

(4) Under VCP stress paths, due to the simultaneous variations in both confining pressure and cyclic deviatoric stress, the amplitude of the pore pressure

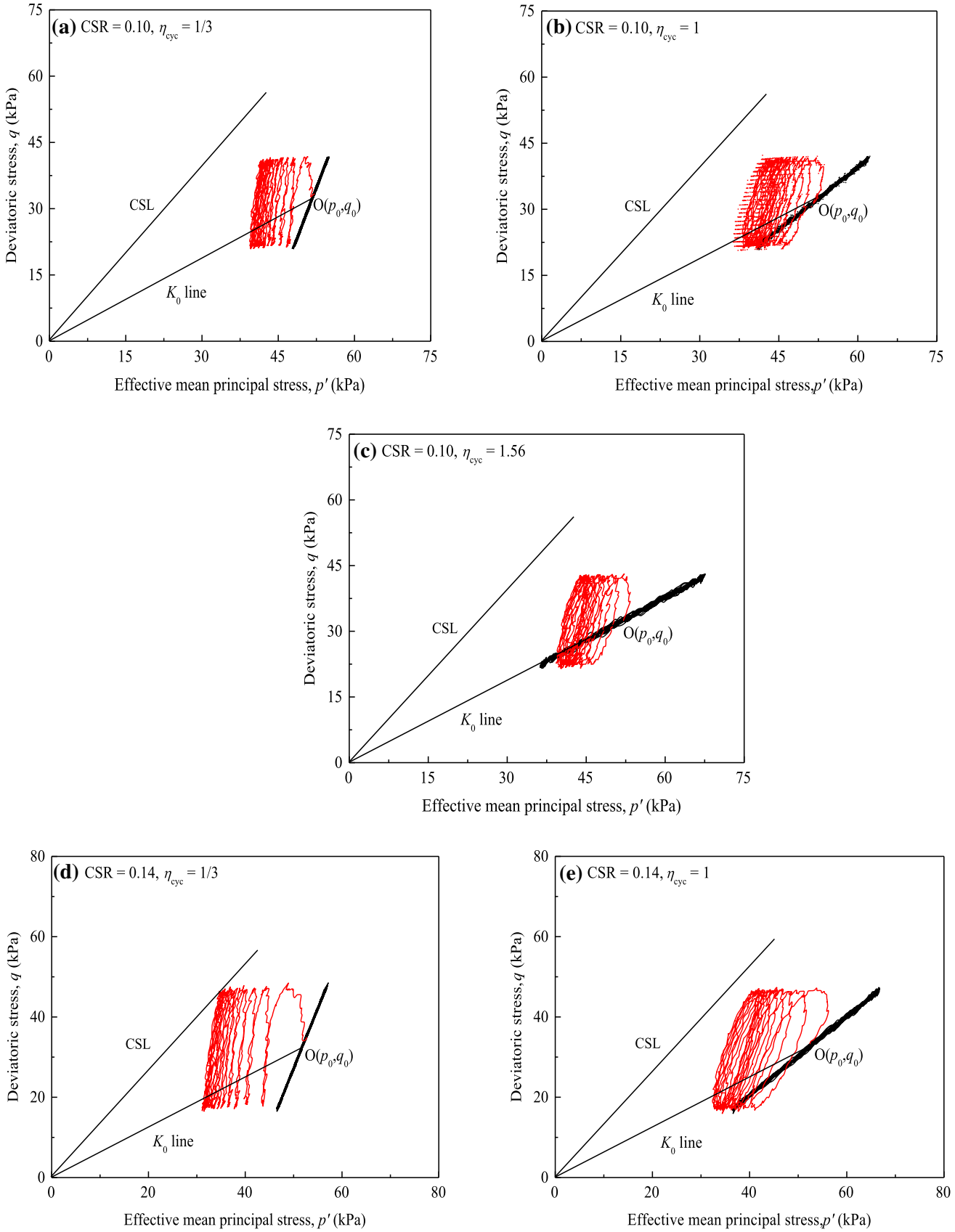

Fig. 13 Effective stress paths of cyclic loading under VCP: **a–c** CSR = 0.10; **d–e** CSR = 0.14; **g–i** CSR = 0.19

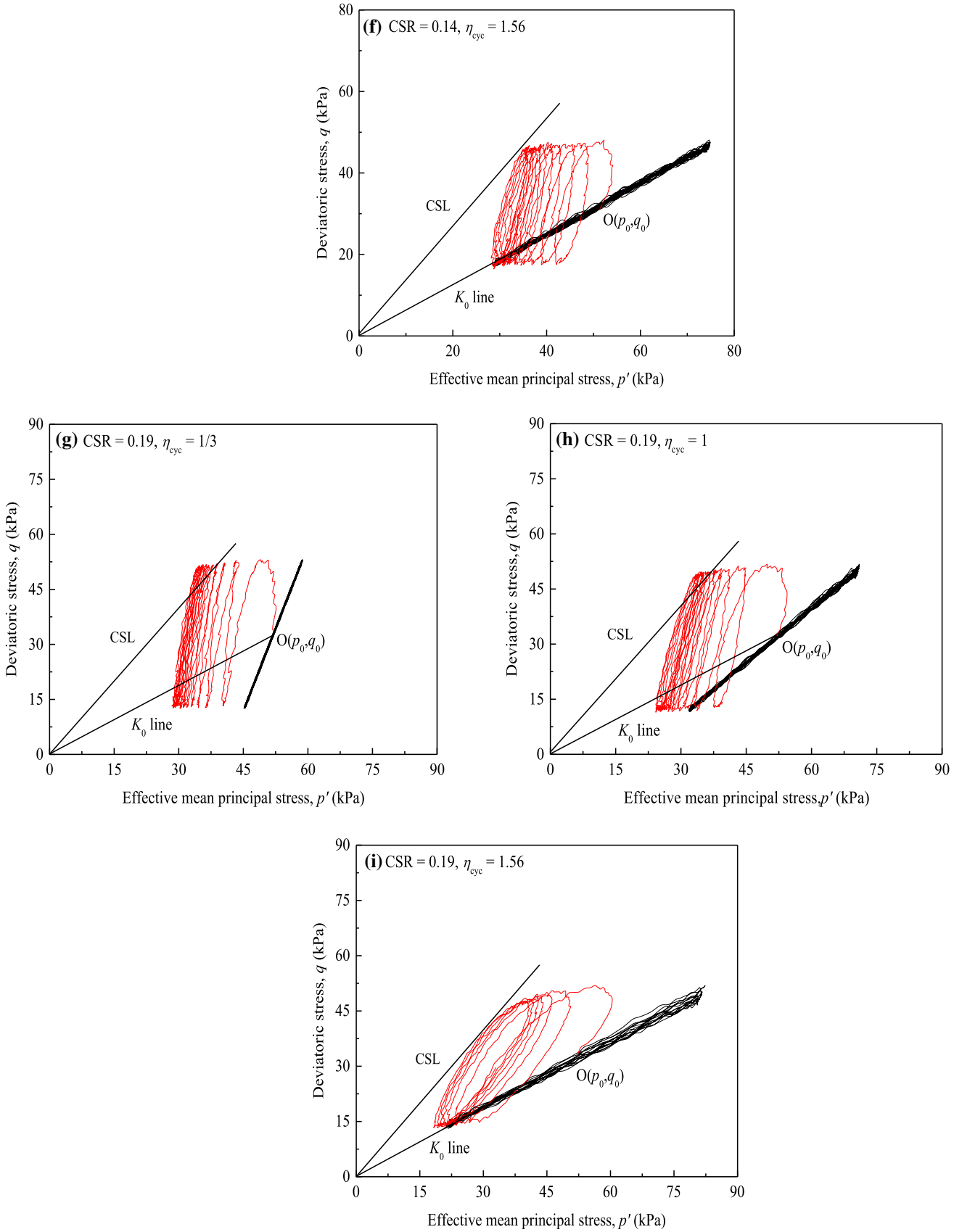

Fig. 13 continued

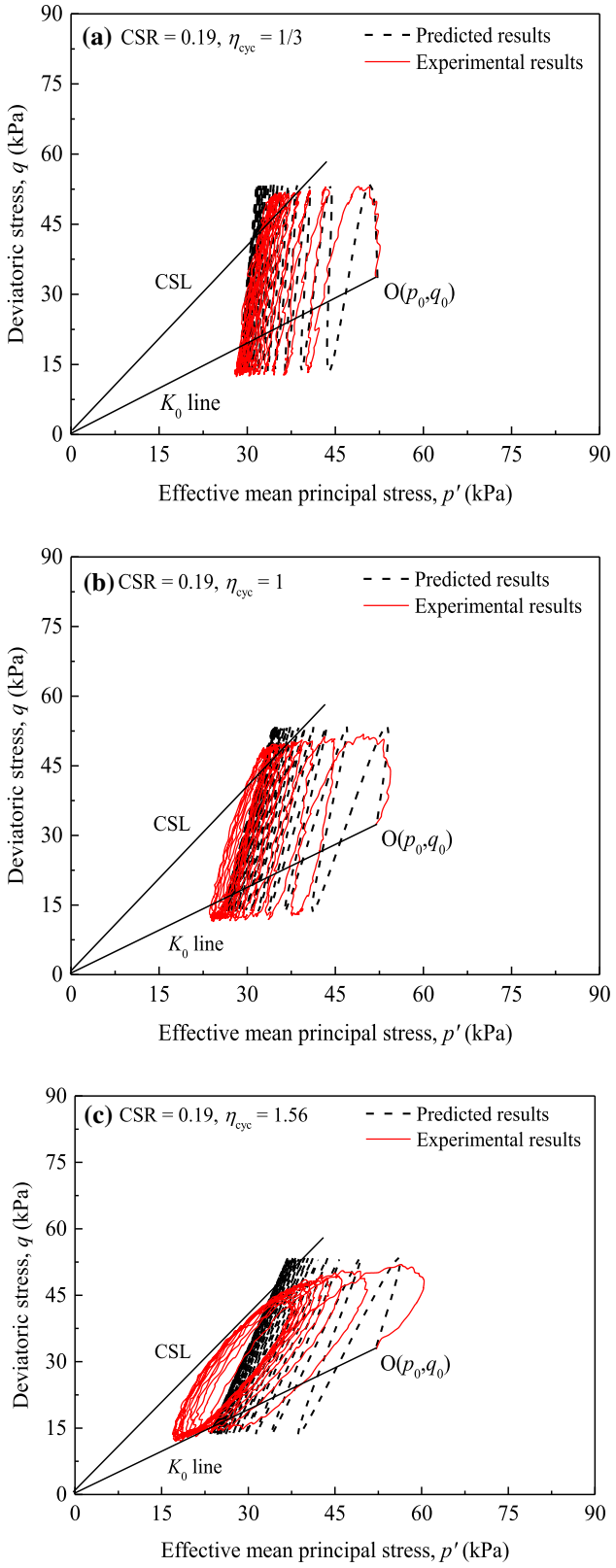

Fig. 14 Predictions of the effective stress paths of cyclic loading under VCP (CSR = 0.19): **a** η_{cyc} = 1/3; **b** η_{cyc} = 1; **c** η_{cyc} = 1.56

is larger, and the effective stress path tilts more sharply to the right. Different effective stress paths are obtained based on the total pore pressure predictions, and these results manifest a relatively good prediction of the effective stress paths under VCP cyclic triaxial tests.

Acknowledgements This research was supported by National Key R&D Program of China (2016YFC0800200), the National Natural Science Foundation of China (Grant No. 51978534, 51778502, 51978532,), the Zhejiang Province Natural Foundation projects of China (Grant No. LR18E080001), Key Research and development program of Zhejiang Province (Grant No. 2018C03038). This financial support is gratefully acknowledged.

References

1. Andersen KH, Pool JH, Brown SF, Rosebrand WF (1980) Cyclic and static laboratory tests on drammen clay. J Geotech Eng Div 106:499–529
2. Cai Y, Gu C, Wang J, Juang CH, Xu C, Hu X (2013) One-way cyclic triaxial behavior of saturated clay: comparison between constant and variable confining pressure. J Geotech Geoenviron Eng 139:797–809. https://doi.org/10.1061/(ASCE)GT.1943-5606.0000760
3. Cai Y, Wu T, Guo L, Wang J (2018) Stiffness degradation and plastic strain accumulation of clay under cyclic load with principal stress rotation and deviatoric stress variation. J Geotech Geoenviron Eng 144:04018021. https://doi.org/10.1061/(asce)gt.1943-5606.0001854
4. Chazallon C, Hornych P, Mouhoubi S (2006) Elastoplastic model for the long-term behavior modeling of unbound granular materials in flexible pavements. Int J Geomech 6:279–289. https://doi.org/10.1061/(ASCE)1532-3641(2006)6:4(279)
5. Gu C, Wang J, Cai Y, Yang Z, Gao Y (2012) Undrained cyclic triaxial behavior of saturated clays under variable confining pressure. Soil Dyn Earthq Eng 40:118–128. https://doi.org/10.1016/j.soildyn.2012.03.011
6. Gu C, Wang J, Cai Y, Sun L, Wang P, Dong Q (2016) Deformation characteristics of overconsolidated clay sheared under constant and variable confining pressure. Soils Found 56:427–439. https://doi.org/10.1016/j.sandf.2016.04.009
7. Gu C, Gu Z, Cai Y, Wang J, Ling D (2017) Dynamic modulus characteristics of saturated clays under variable confining pressure. Can Geotechn J 54:729–735. https://doi.org/10.1139/cgj-2016-0441
8. Guo L, Wang J, Cai Y, Liu H, Gao Y, Sun H (2013) Undrained deformation behavior of saturated soft clay under long-term cyclic loading. Soil Dyn Earthq Eng 50:28–37. https://doi.org/10.1016/j.soildyn.2013.01.029
9. Guo L, Cai Y, Jardine RJ, Yang Z, Wang J (2018) Undrained behaviour of intact soft clay under cyclic paths that match vehicle loading conditions. Can Geotech J 55:90–106. https://doi.org/10.1139/cgj-2016-0636
10. Li LL, Dan HB, Wang LZ (2011) Undrained behavior of natural marine clay under cyclic loading. Ocean Eng 38:1792–1805. https://doi.org/10.1016/j.oceaneng.2011.09.004
11. Lunne T, Berre T, Andersen KH, Strandvik S, Sjursen M (2006) Effects of sample disturbance and consolidation procedures on measured shear strength of soft marine Norwegian clays. Can Geotech J 43:726–750. https://doi.org/10.1139/T06-040

12. Nataatmadja A, Parkin AK (1989) Characterization of granular materials for pavements. Can Geotech J 26:725–730. https://doi.org/10.1139/t89-083
13. Rondón HA, Wichtmann T, Triantafyllidis T, Lizcano A (2009) Comparison of cyclic triaxial behavior of unbound granular material under constant and variable confining pressure. J Transp Eng 135:467–478. https://doi.org/10.1061/(ASCE)TE.1943-5436.0000009
14. Simonsen E, Isacsson U (2001) Soil behavior during freezing and thawing using variable and constant confining pressure triaxial tests. Can Geotech J 38:863–875. https://doi.org/10.1139/cgj-38-4-863
15. Skempton AW (1954) The pore-pressure coefficients a and b. Geotechnique 4:143–147. https://doi.org/10.1680/geot.1954.4.4.143
16. Sun Q, Cai Y, Chu J, Dong Q, Wang J (2017) Effect of variable confining pressure on cyclic behaviour of granular soil under triaxial tests. Can Geotech J 54:768–777. https://doi.org/10.1139/cgj-2016-0439
17. Wang J, Guo L, Cai Y, Xu C, Gu C (2013) Strain and pore pressure development on soft marine clay in triaxial tests with a large number of cycles. Ocean Eng 74:125–132. https://doi.org/10.1016/j.oceaneng.2013.10.005
18. Wang YK, Guo L, Gao YF, Qiu Y, Hu XQ, Zhang Y (2016) Anisotropic drained deformation behavior and shear strength of natural soft marine clay. Marine Georesources Geotechnol 34:493–502. https://doi.org/10.1080/1064119X.2015.1081653
19. Wichtmann T, Niemunis A, Triantafyllidis T (2007) On the influence of the polarization and the shape of the strain loop on strain accumulation in sand under high-cyclic loading. Soil Dyn Earthq Eng 27:14–28. https://doi.org/10.1016/j.soildyn.2006.05.002
20. Yasuhara K, Yamanouchi T, Hirao K (1982) Cyclic strength and deformation of normally consolidated clay. Soils Found 22:77–91. https://doi.org/10.3208/sandf1972.22.3_77
21. Zaman M, Chen DH, Laguros J (1994) Resilient moduli of granular materials. J Transp Eng 120:967–988. https://doi.org/10.1061/(ASCE)0733-947X(1994)120:6(967)
22. Zeng LL, Chen XP (2009) Analysis of mechanical characteristics of soft soil under different stress paths. Yantu Lixue/Rock Soil Mech 30:1264–1270
23. Zergoun M, Vaid YP (1994) Effective stress response of clay to undrained cyclic loading. Can Geotech J 31:714–727. https://doi.org/10.1139/t94-083
24. Zhang JM, Xie DY (1993) Research progress in theory and application of vibration and gap water pressure of saturated sand. J Hydraul Eng 50:165–180